Vol. 25, No. 3(2026) Sim26874

Revista Mexicana de Ingeniería Química

Experimental implementation of MPC strategy by manipulating the stirring speed to control secondary nucleation in continuous crystallization

Implementación experimental de una estrategia MPC manipulando la velocidad de agitación para controlar la nucleación secundaria en un cristalizado continuo

M. Presenda-de Dios[1], A. Reyes-Obando[1], L. A. Ricardez-Sandoval[2], P. A. Quintana-Hernández[1]*

[1]Departamento de Ingeniería Química, TecNM en Celaya, García Cubas Pte # 600, Celaya, Guanajuato, México, 38010

[2]Department of Chemical Engineering, University of Waterloo, 200 University Avenue West, Waterloo, N2L 3G1, Waterloo, Canada.

Received: May 19, 2026; Accepted: August 10, 2026

Abstract

This paper presents the experimental implementation of a multivariable model predictive control (MPC) for the continuous crystallization of ammonium sulfate in a Mixed-Suspension, Mixed-Product-Removal (MSMPR) crystallizer. The strategy employs a dynamic model based on balances of mass, energy and population and coordinates stirring speed and coolant flow as manipulated variables for the simultaneous control of average crystal diameter D(4,3) and the crystallizer temperature. This multivariable control strategy is innovative because incorporates hydrodynamics effects on mechanically induced secondary nucleation. The experiments were conducted in a pilot plant equipped with Process Analytical Technology (PAT) for online monitoring of Crystal Size Distribution (CSD), temperature and solution concentration. The results demonstrated that the MPC was able to maintain operation within the metastable zone, reduced process oscillations, and improved setpoint tracking. Furthermore, the implementation of digital filtering and the adjustment of predictive horizons reduced the error associated with the CSD and stabilized control actions, validating the feasibility of the active use of agitation in the control of continuous crystallization systems.

Keywords: multivariable control, crystallization, ammonium sulfate, secondary nucleation, metastable zone operation.

Resumen

Este trabajo presenta la implementación experimental de un controlador predictivo basado en un modelo (MPC) multivariable para la cristalización continua de sulfato de amonio en un cristalizador Mixed-Suspension, Mixed-Product-Removal (MSMPR). La estrategia emplea un modelo dinámico basado en balances de materia, energía y población y coordina la velocidad de agitación y el flujo de refrigerante como variables manipuladas para el control simultáneo del diámetro promedio de cristales D(4,3) y la temperatura del cristalizador. Esta estrategia de control multivariable es innovadora porque incorpora efectos hidrodinámicos en la nucleación secundaria inducidos mecánicamente. Los experimentos se realizaron en una planta piloto equipada con Tecnología Analítica de Procesos (PAT) para el monitoreo en línea de la Distribución de Tamaño de cristal (CSD), temperatura y concentración de la solución. Los resultados demostraron que el controlador MPC pudo mantener la operación dentro de la zona metaestable, reducir las oscilaciones y mejorar el seguimiento hacia el punto de referencia. Además, la implementación de filtrado digital y el ajuste de los horizontes predictivos permitieron disminuir el error asociado a la CSD y estabilizar las acciones de control, validando la viabilidad del uso activo de la agitación en sistemas de cristalización continua.

Palabras clave: control multivariable, cristalización, sulfato de amonio, nucleación secundaria, operación en la zona metaestable.

*Corresponding author. *E-mail*: pedro@iqcelaya.itc.mx ;
https://doi.org/10.24275/rmiq/Sim26874
ISSN:1665-2738, *issn-e*: 2395-8472

1 Introduction

Industrial crystallization is one of the most widely used unit operations for separation and purification in the chemical, pharmaceutical, and agrochemical industries. The quality of the final product is directly linked to the Crystal Size Distribution (CSD), since the average diameter and morphology of the crystals determine critical properties such as dissolution rate, solid purity, and the efficiency of subsequent operations such as filtration, washing, and drying (Larson & Mullin, 1973; Tadayon *et al*., 2002). In systems used industrially to produce fertilizers such as ammonium sulfate, precise control of the CSD is of particular importance given its direct impact on the product's handling and marketability (Peng *et al*., 2024).

In recent decades, the chemical and pharmaceutical industries have driven a strategic transition from batch processes to continuous manufacturing systems, motivated by numerous advantages such as greater product homogeneity, reduced batch-to-batch variability, lower operating costs, and real-time access to process data (Fisher *et al*., 2022; Lee *et al*., 2015). Within these continuous configurations, mixed-suspension mixed-product-removal (MSMPR) crystallizers have gained significant prominence as a benchmark technology due to their ease of adaptation from existing stirred-tank reactors and their compatibility with moderate crystallization kinetics (Diab & Gerogiorgis, 2017; Zhao *et al*., 2023). Comparative studies have shown that MSMPR systems offer more stable and controlled production compared to batch processes, although achieving steady-state conditions requires robust control strategies (Stoffan *et al*., 2024).

Controlling MSMPR systems poses a significant engineering challenge, primarily due to the highly nonlinear nature of nucleation and growth kinetics, which are interrelated through supersaturation as the driving force (Lima *et al*., 2022; Wang *et al*., 2023). In the absence of adequate control, the process may exhibit persistent oscillations in the CSD or drifts out of the metastable zone, causing uncontrolled primary nucleation and the production of an out-of-specification product (Moldoványi *et al*., 2005). Historically, the regulation of these processes has relied on open-loop strategies or PID controllers to stabilize the temperature, without fully leveraging the available information on the crystalline population.

The emergence of Process Analytical Technologies (PAT), such as focused beam reflectance (FBRM), attenuated total reflectance infrared spectroscopy (ATR-FTIR), and in-line imaging, has transformed the possibilities for real-time monitoring and control of crystallization processes (Zhao *et al*., 2023; Wu *et al*., 2015). These tools enable the continuous measurement of variables such as string distribution, solute concentration, and temperature, facilitating the development of much more sophisticated model-based control strategies (Gao *et al*., 2021). However, their implementation in industrial and pilot environments faces the problem of instrumental noise generated, for example, by air bubbles or sensor fouling, which requires the design of digital filtering strategies that ensure the stability of the control loop.

Model Predictive Control (MPC) has been used as one of the most robust tools for addressing these challenges. Unlike classical control schemes, MPC explicitly handles multivariable systems, compensates for delays inherent in-residence time, and accounts for operational constraints on both actuators and output variables (Qin & Badgwell, 2003). Previous research has explored the use of MPC and its nonlinear variants (NMPC) to optimize CSD in batch and continuous processes, focusing primarily on manipulating the temperature or cooling profile as the manipulated variable (Cao *et al*., 2017; Sun *et al*., 2024; Wang *et al.,* 2023). However, most of these studies have been limited to simulation environments or batch systems, often overlooking the complexity of experimental implementation in continuous MSMPR-type crystallizers.

The work by Moldoványi *et al*. (2005) demonstrated the feasibility of linear MPC for MSMPR crystallizers in simulation, using the method of moments for population balance. Subsequently, the trend toward NMPC gained traction due to increases in available computational capacity (Lima *et al*., 2022). Recent research, such as that by Lima *et al*. (2025), has proposed robust methodologies for implementing experimental NMPC by combining population balance models with PAT sensors and state estimators based on artificial neural networks, achieving promising results in batch processes for paracetamol. Similarly, studies such as that by Wang *et al*. (2023) propose NMPC strategies combined with image analysis for simultaneous control of crystal size and distribution in alumina. However, experimental implementation in MSMPR-type continuous crystallizers for systems of agronomic value remains scarce in the literature.

A critical gap identified in the current state of the art is the limited use of hydrodynamics as an active control variable. Although it is widely recognized that agitation intensity not only ensures the suspension of solids but is also the fundamental driver of secondary nucleation via mechanical contact (Yousuf & Frawley, 2019; Li *et al*., 2020). Few studies have integrated agitation rate as a coordinated manipulated variable in an experimental MPC scheme. Secondary nucleation induced by contact between crystals and the agitator, and between crystals and the

equipment walls, is the dominant mode in industrial stirred crystallizers according to Mullin (2001), and its rate is directly correlated with the agitation rate and the suspension density, as indicated by Bal and Peters (2020). Detailed hydrodynamic studies have shown that controlling the agitation rate modifies the particle size distribution through its effect on turbulent shear stress and the secondary nucleation rate (Yousuf & Frawley, 2019). Recent studies specifically on ammonium sulfate crystallization have confirmed that hydrodynamic parameters and stirring geometry significantly influence both nucleation rates and crystal growth size (Xiong *et al*., 2025), reinforcing the physical rationale for incorporating agitation into continuous control schemes

The development of computationally efficient models capable of running in real time is another ongoing challenge in this field. The method of moments, applied to population balance, offers a reduced representation of the system that transforms the complex set of integrodifferential equations of the population balance into a system of low-order ordinary differential equations, suitable for integration into a real-time MPC scheme (Moldoványi *et al*., 2005). Recently, complementary strategies such as the use of digital twins have been proposed to improve the system's predictability and directly control nucleation (Leeming *et al*., 2023), although the experimental validation of these approaches under instrumental noise conditions remains an active area of research.

This study addresses this issue through the experimental implementation of a multivariable MPC controller in an MSMPR-type continuous crystallization pilot plant for the ammonium sulfate-water system. The central contribution of this research lies in the simultaneous control of the crystallizer temperature and the average CSD (diameter D(4,3)), using both the coolant flow rate and the agitation speed as manipulated variables in a coordinated and proactive manner. This approach allows for balancing the thermal and mechanical effects on crystal formation, systematically exploiting the phenomenon of secondary nucleation as a mechanism for controlling CSD. Additionally, a moving-average filter and a sequential experimental adjustment of selected MPC tuning parameters were evaluated to reduce the impact of PAT measurement noise and improve the trade-off between setpoint tracking and actuator activity.

2 Methodology

2.1 *Model of the crystallization process*

A general model that describes a continuous crystallization process can be formulated as a set of ordinary differential equations (ODEs). This model includes a population balance (a partial differential equation reduced to a set of ordinary differential equations using the method of moments, a mass balance of the solute dissolved in the solvent, and two energy balances, one corresponding to the crystallizer and the other to the jacket. These equations can be simplified based on considerations specific to an MSMPR-type (Quintana-Hernández *et al*., 2017; Medina-Galván *et al*., 2020). The following expressions present the differential equations that constitute the model along with the constitutive equations for nucleation and growth reported previously by Tututi-Avila (2010) and Reyes-Obando (2012).

$$\frac{d\mu_0}{dt} = \frac{\mu_0^e - \mu_0}{\tau} + B, \tag{1}$$

$$\frac{d\mu_j}{dt} = \frac{\mu_j^e - \mu_j}{\tau} + jG\mu_{j-1} \qquad j = 1,2,..,5, \tag{2}$$

$$\frac{dC}{dt} = \frac{\varepsilon_e C_e - C + k_v C \mu_3^e - 3\tau k_v G \mu_2 (\rho_c - C)}{\tau(1 - k_v \mu_3)}, \tag{3}$$

$$\frac{dT}{dt} = \frac{\rho Q C_p (T_e - T) - UA(T - T_c) - 3\Delta H_c \rho_c k_v V G \mu_2}{\rho V C_p}, \tag{4}$$

$$\frac{dT_c}{dt} = \frac{\rho_a q C_{pa} (T_r - T_c) + UA(T - T_c) - U_0 A_0 (T_c - T_\infty)}{\rho_a V_c C_{pa}}, \tag{5}$$

$$B = k_b (1 - k_v \mu_3) S_r^b M_t^o N_r^p \tag{6}$$

$$G = k_g S_r^g (446 - 0.3515 N_r)^h. \tag{7}$$

In Equations (1–7), t represents time, τ denotes the residence time in the crystallizer, and μ_j corresponds to the j-th moment of the crystal size distribution (for $j = 0,\ldots,5$), where $\mu_{j,e}$ signifies the j-th moment in the feed stream. The terms B and G express the overall secondary nucleation rate and crystal growth rate, respectively. In the solute mass balance (Eq. 3), C is the solute concentration in the liquid phase, C_e is the feed solute concentration, ε_e represents the solid-free phase in the feed, k_v is the volumetric crystal shape factor, and ρ_c is the density of the crystal solid. For the crystallizer energy balance (Eq. 4), T is the slurry temperature, T_e is the feed solution temperature, ρ is the solution density, Q is the volumetric feed flow rate, C_p is the solution heat capacity, V is the operational crystallizer volume, U and A are the heat transfer coefficient and area between the crystallizer and the jacket, T_c is the jacket coolant temperature, and ΔH_c represents the enthalpy of crystallization. In the jacket energy balance (Eq. 5), q denotes the coolant volumetric flow rate, T_r is the inlet coolant temperature, ρ_a and C_{pa} are the density and heat capacity of the coolant, V_c is the cooling jacket volume, T_∞ is the ambient temperature, while U_0 and A_0 represent the heat transfer coefficient and

area between the jacket and the surroundings. In the kinetic constitutive expressions (Eqs. 6–7), k_b and k_g are the kinetic constants for nucleation and growth, S_r denotes the relative supersaturation, b and g are the kinetic orders with respect to supersaturation, M_t is total mass of crystals (where $M_t = \rho_c k_v \mu_3$), o is the power exponent for suspension density, N_r is the stirring speed, p is the empirical exponent accounting for mechanically induced secondary nucleation, and h is the exponent associated with agitation speed in growth kinetics.

To explicitly evaluate the driving force of crystallization embedded in the kinetic expressions and establish the experimental operating range, Equations (8–10) define the thermodynamic saturation boundaries and physical property correlations for the ammonium sulfate–water system. Specifically, C_{Sat} in Eq. (8) denotes the saturation concentration as a function of temperature (Perry & Green, 1997), defining the equilibrium limit required for supersaturation calculations. In Eq. (9), C_z represents the metastable limit concentration (Lugo-Martínez, 2005), which establishes the upper boundary of the metastable zone width beyond which primary nucleation spontaneously occurs. Furthermore, Eq. (10) provides an empirical relationship to indirectly infer solution concentration from real-time online measurements of temperature and solution density (Enríquez-Torres, 2005). The empirical parameters determined for the ammonium sulfate–water system are summarized in Table 1.

$$C_{Sat} = 1.052 \times 10^{-5} T^2 + 2.236 \times 10^{-3} + 0.7055, \quad (8)$$

$$C_z = 1.3178 \times 10^{-7} T^3 + 2.6136 \times 10^{-6} T^2 + 2.6280 \times 10^{-3} T + 0.7076, \quad (9)$$

$$C = -5.9107 + 1.9811 \times 10^{-3} T + 5.3275 \rho. \quad (10)$$

Building upon the dynamic moment balances and concentration relationships, Equations (11–13) define the explicit dynamic evolution of the primary target variable for particle size control. Equation (11) evaluates the volume-weighted mean crystal diameter $D(4,3)$, calculated as the ratio between the fourth (μ_4) and third (μ_3) moments of the crystal distribution based on the volume of crystals in solution. Since no direct dynamic equation exists for this mean, applying the chain rule to Eq. (11) yields its time derivative, $\frac{dD(4,3)}{dt}$, as formulated in Eq. (12). Finally, solving Eq. (2) for μ_3 and μ_4 and substituting these dynamic moment expressions into Eq. (12) yields the final dynamic equation, Eq. (13), which explicitly details how crystal growth kinetics, residence time, and lower-order distribution moments dynamically dictate the temporal evolution of the average crystal size.

$$D(4,3) = \frac{\mu_4}{\mu_3}, \quad (11)$$

$$\frac{dD(4,3)}{dt} = \frac{dD(4,3)}{d\mu_3}\left(\frac{d\mu_4}{dt}\right) + \frac{dD(4,3)}{d\mu_4}\left(\frac{d\mu_3}{dt}\right) \quad (12)$$

$$\frac{dD(4,3)}{dt} = \frac{1}{\mu_3}\left(\frac{\mu_4^e}{\tau} - \frac{\mu_4}{\tau} + 4\mu_3 G\right) - \frac{\mu_4}{\mu_3^2}\left(\frac{\mu_3^e}{\tau} - \frac{\mu_3}{\tau} + 3\mu_2 G\right). \quad (13)$$

2.2 MPC Model

To achieve simultaneous regulation of the crystal size distribution and process temperature, a multivariable Quadratic Dynamic Matrix Control (MPC-QDMC) formulation was implemented using the MATLAB® Model Predictive Control Toolbox. This framework calculates an optimal predictive control law for constrained multivariable systems by casting the control objective into an online optimization problem solved at each sampling time, T_s, via Quadratic Programming (QP). The resulting objective function and its associated operational constraints are defined by Eq. (14):

Table 1. Physical and kinetic parameters used in the crystallization model.

Parameter	Value	Parameter	Value
b	0.562 (-)	C_e	0.763 $g\ g^{-1}$
g	1.500 (-)	T_e	38.4 °C
h	1.337 (-)	T_r	Tsat -4°C
k_b	180.0 # $g^{-o} cm^{3o-3}\,\mathrm{min}^{-1}\,rpm^{-p}$	T_∞	25.0 °C
k_g	9.09 ×10^{-4} $cm\ min^{-1} rpm^{-h}$	$(UA)_\infty$	100 ($cal\ min^{-1} {}^\circ C^{-1}$)
k_v	4*pi/3 (-)	V	3000 cm^{-3}
o	0.001 (-)	V_c	820.0 cm^{-3}
p	0.050 (-)	ε_e	0.98 (-)
ρ_c	1.769 $g\ cm^{-3}$	τ	10.0 (min)
C_p	0.39 $cal\ g^{-1}\ {}^\circ C^{-1}$	ΔH_c	-0.136 T-7.54 ($cal\ g^{-1}$)

$$\Delta u(k|k),...,\Delta u(k+H_c-1|k),\alpha \sum_{i=0}^{H_{p-1}} \left(\sum_{j=1}^{\min_{n_y}} \left| W^{y}_{i+1,j} \left(y_j(k+i+1|k) - r_j(k+i+1) \right) \right|^2 + \sum_{j=1}^{n_u} \left| W^{\Delta u}_{i,j} \Delta u(k+i|k) \right|^2 \right) + \lambda \alpha^2 \tag{14}$$

subject to:

$$u_{j,\min}(i) - \alpha V^{u}_{j,\min}(i) \le u_j(k+i|k) \le u_{j,\max}(i) + \alpha V^{u}_{j,\max}(i)$$
$$\Delta u_{j,\min}(i) - \alpha V^{\Delta u}_{j,\min}(i) \le \Delta u_j(k+i|k) \le \Delta u_{j,\max}(i) + \alpha V^{\Delta u}_{j,\max}(i)$$
$$y_{j,\min}(i) - \alpha V^{y}_{j,\min}(i) \le y_j(k+i+1|k) \le y_{j,\max}(i) + \alpha V^{y}_{j,\max}(i)$$
$$\Delta u(k+h|k) = 0$$
$$\alpha \ge 0$$

for:

$$i = 0,\ldots,H_{p-1}$$
$$h = H_c,\ldots,H_{p-1}$$

In Equation (14), the model predictive controller recursively minimizes a scalar objective function at each sampling step k with respect to the decision variables: the sequence of control move increments $\{\Delta u(k|k),\ldots,\Delta u(k+H_c-1|k)\}$ and the slack variable α. The tuning parameters H_p and H_c correspond to the prediction horizon and control horizon, respectively, whereas n_y represents the number of output variables and n_u denotes the number of manipulated inputs. The index i ($i = 0,\ldots,H_p-1$) spans the prediction horizon. Within the objective function, $y_j(k+i+1|k)$ represents the predicted j-th output variable at future step $k+i+1$ calculated at time k, $r_j(k+i+1)$ is the corresponding reference trajectory setpoint, and $W^{y}_{i+1,j}$ is the weighting factor for output tracking errors. Furthermore, $\Delta u_j(k+i|k)$ represents the control move increment for the j-th manipulated input at step i, weighted by $W^{\Delta u}_{i,j}$. The term $\lambda\alpha^2$ introduces a penalty factor λ on the slack variable α to prevent excessive constraint violations while ensuring optimization feasibility. The minimization problem is subject to soft constraints for the manipulated inputs $u_j(k+i|k)$, control move increments $\Delta u_j(k+i|k)$, and predicted outputs $y_j(k+i+1|k)$. These variables are bounded by lower and upper limits ($u_{j,\min}$, $u_{j,\max}$, $\Delta u_{j,\min}$, $\Delta u_{j,\max}$, $y_{j,\min}$, $y_{j,\max}$), which are relaxed using the slack variable α weighted by their respective violation severity parameters ($V^{u}_{j,\min}$, $V^{u}_{j,\max}$, $V^{\Delta u}_{j,\min}$, $V^{\Delta u}_{j,\max}$, $V^{y}_{j,\min}$, $V^{y}_{j,\max}$). Finally, the condition $\Delta u(k+h|k) = 0$ forces the control move increments to zero beyond the control horizon ($h = H_c,\ldots,H_p-1$), and $\alpha \ge 0$ guarantees the non-negativity of the slack variable.

To establish a baseline for optimal setpoint tracking, the initial controller parameters and weighting values were determined offline through simulation of the continuous crystallizer.

Table 2. MPC controller tuning parameters and weights, obtained through simulation of a crystallization model.

Parameters	values
Prediction horizon, H_p	30
Control horizon, H_c	10
Sampling time	5 min
Weights	**Values**
Stirring, $W^{\Delta U}_1$	5
Flow water, $W^{\Delta U}_2$	5
Temperature, W^{y}_1	700
D(4,3), $W^{\Delta Uy}_2$	88,000

This preliminary tuning aimed to minimize settling time for both temperature and crystal size distribution (CSD). The resulting parameters and weights are summarized in Table 2, while Figure 1 displays the dynamic response curves to step changes in setpoints.

These simulation-derived values served as initial inputs for the predictive controller, which operates as a digital twin to correct deviations by manipulating final control elements and minimizing squared tracking errors. However, to accommodate unmodeled physical delays, measurement noise, and actuator limits inherent in the pilot plant, the prediction and control horizons were further refined during real-time operation. This online adjustment ensured prompt setpoint recovery across different experimental conditions without overstressing physical equipment.

2.3 Equipment

Figure 2 shows the continuous pilot plant used for the crystallization of ammonium sulfate (Pilot Unit No. 9312122, Pignat, France). It includes a 3000 cm^3 crystallizer cooled by a LAUDA RP1800 thermal bath (Lauda-König, Schofen, Germany). The equipment features a 40-L stirred and heated tank for preparing the feed solution.

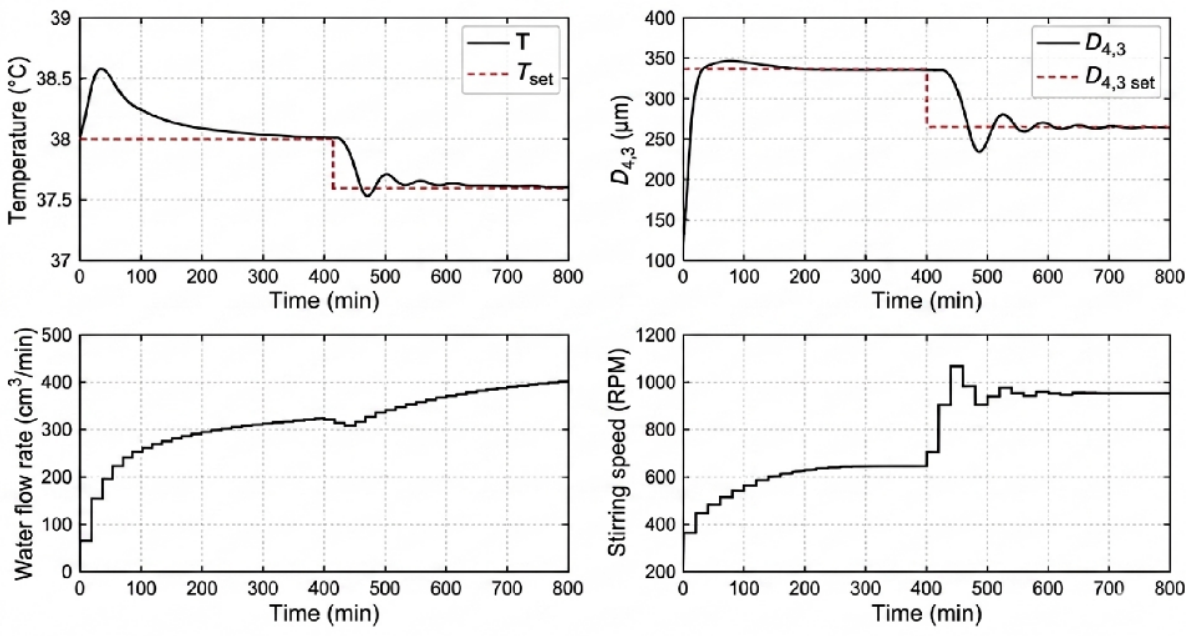

Figure. 1. Simulation of the crystallization process controlled by MPC.

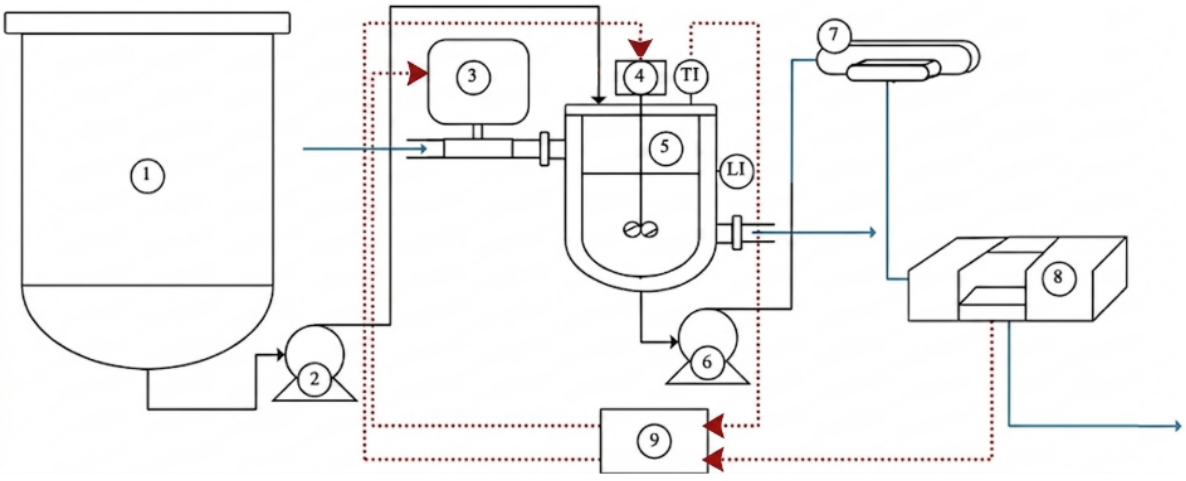

Figure. 2. Diagram of the pilot plant used for the experimental tests: 1) solution preparation tank, 2) and 6) peristaltic pumps, 3) solenoid valve for controlling the coolant flow, 4) stirrer, 5) crystallizer, 7) densitometer, 8) particle size analyzer, and 9) data acquisition system and MPC controller. The solid black lines represent the solution flow, the solid blue lines represent the coolant flow, and the red dashed lines represent the input and output signals of the controller.

The analytical system consists of an mPDS200 densitometer for continuous monitoring of density (Anton Paar, Austria); a Mastersizer for continuous particle size analysis (Malvern Instruments Ltd, England) and a DAQ-USB 9401 signal acquisition and generation system (National Instruments, USA) is used, with NI-9211 modules for analog recording and NI-9265 modules for current generation, integrated via LabVIEW and DAVIS software.

2.4 Experimental methodology

A saturated solution of ammonium sulfate was prepared in a 40-L tank at 38.4 °C, ensuring complete dissolution of the solid phase through thermal conditioning until the saturation temperature (Tsat) was reached. Subsequently, 1% w/w of crystalline seeds were added and calculated based on the operating volume and the density of the solution, with an average crystal size (CSD) of 113 μm. Prior to inoculation, the system was recirculated to adjust the baseline of the particle analyzer.

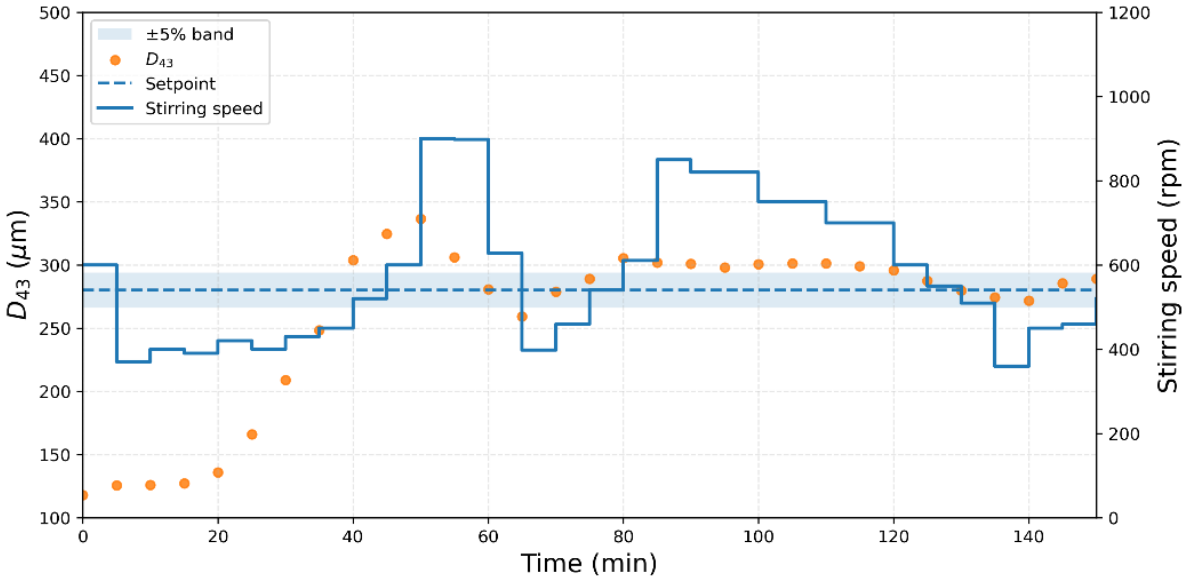

Figure 3. CSD– agitation control loop.

After adding the seeds, the initial particle size characterization was performed under a recirculation flow of 500 cm^3/min. The suspension was then fed into the crystallizer via a peristaltic pump at a flow rate of 250 cm^3/min, maintaining a constant operating volume of 2500 cm^3. Stirring was set to 300 rpm, and cooling was initiated using a coolant flow rate of 400 cm^3/min at a temperature four degrees below the saturation temperature to ensure operation conditions within the metastable zone width.

3 Results and discussion

Three different experiments were performed, changing the MPC parameters. The first case analyzed the closed-loop experiment using the MPC controller. It was set with a reference temperature of 36.4°C and a mean crystal size of 280 μm (with a stability range of 266 to 294 microns). The mean size of the seeds used was 113 μm, and the solution feed temperature was 38.7°C. The control loop dynamics between the average crystal size and the stirring speed are shown in Figure 3. During the first 40 minutes, crystal growth is observed at a low stirring speed. When the average crystal size exceeds the set point, the stirring speed increases, resulting in a reduction in the average crystal size because higher speed promotes the breakage of large crystals due to mechanical contact. The system reaches steady-state operation defined within ±5% of the operating point around minute 130. Some adjustments to the MPC parameters must be made to accelerate the response.

Figure 4 shows the process temperature profile. With the selected MPC parameters, the desired temperature value was reached very fast. The coolant flow rate does not have a strong control demand. Temperature remained stable after 70 minutes of operation without any fluctuations and ensured that the process operates within the metastable zone. Figure 5 shows the behavior of the ammonium sulfate concentration in the crystallizer; note that the operating band of the metastable zone is a very narrow region, from which the system can easily deviate if proper control is not maintained. In this case, the MPC controller was able to maintain system operation within the metastable zone.

The second experiment used the same initial values as the previous one, but the MPC controller weights $W_1^{\Delta U}$ and $W_2^{\Delta U}$ were changed from 5 to 2 so that the actuators could make faster adjustments and reduce the overshoot that occurred in the first experiment.

By implementing changes to the controller's parameters and limits, the overshoot was reduced, and it can be observed that changes in the manipulated variables occur more frequently. Figure 6 shows the time evolution of D(4,3) and the stirring speed. The main difference of this experiment is that the controller responds faster to deviations from the setpoint, generating smooth changes when disturbances are small and more aggressive actions when the system deviates significantly from the reference.

Figure 7 shows the response of the temperature and refrigerant flow under the new controller configuration. Although the tracking of the D(4,3) setpoint improved, the system exhibited greater variability in control actions, particularly in the refrigerant flow. This demonstrates that an excessive reduction in weights can significantly increase the controller's aggressiveness and result in greater operational stress on the actuators.

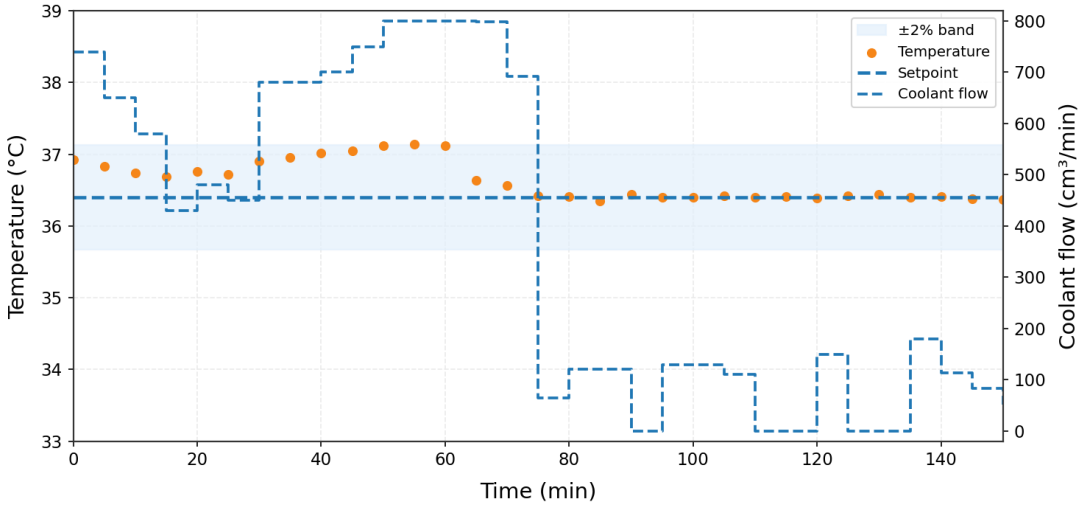

Figure 4. Temperature-Water Flow Control Loop.

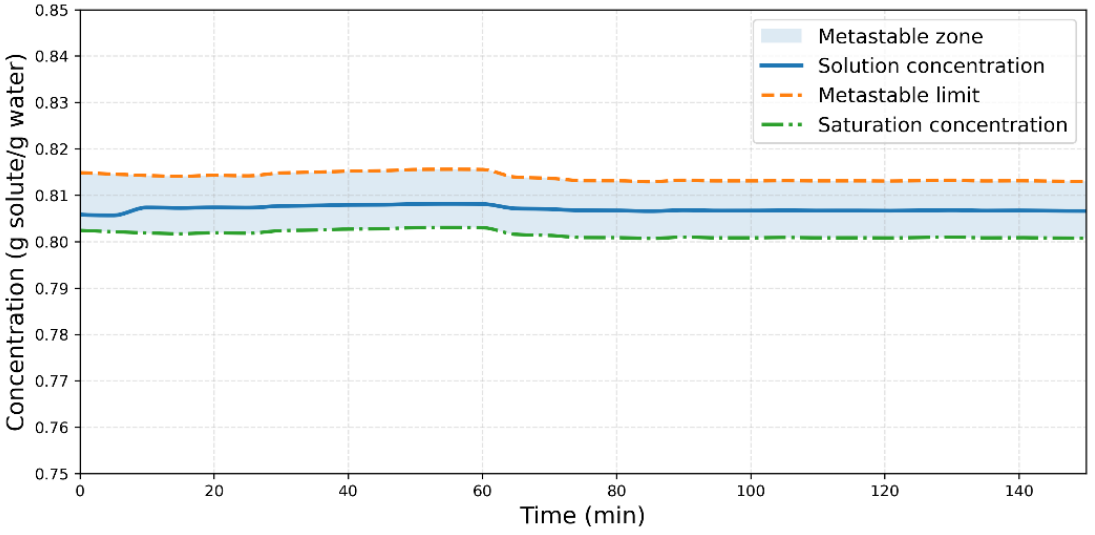

Figure 5. Concentration profile inside the crystallizer

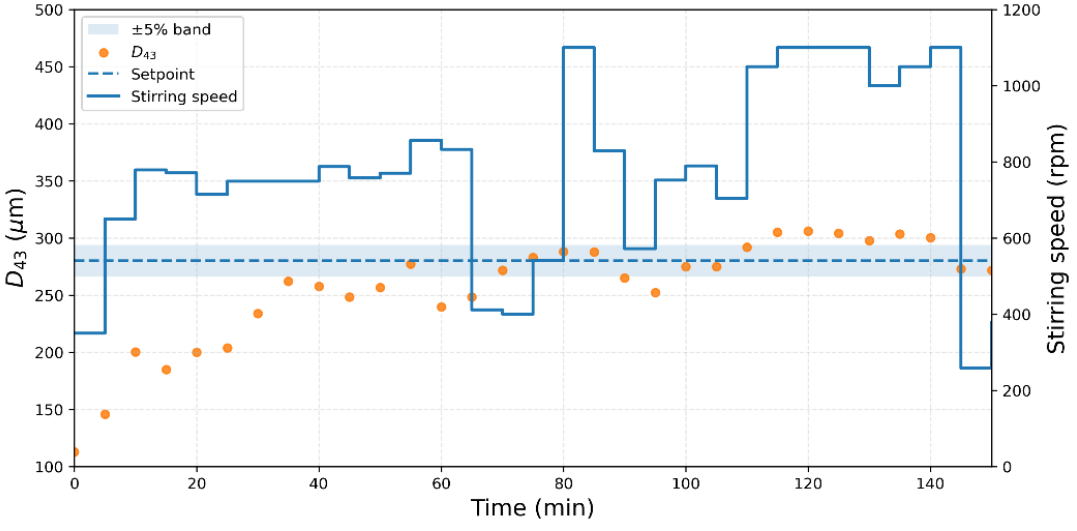

Figure 6. D(4,3)—Stirring control loop, using the new weights

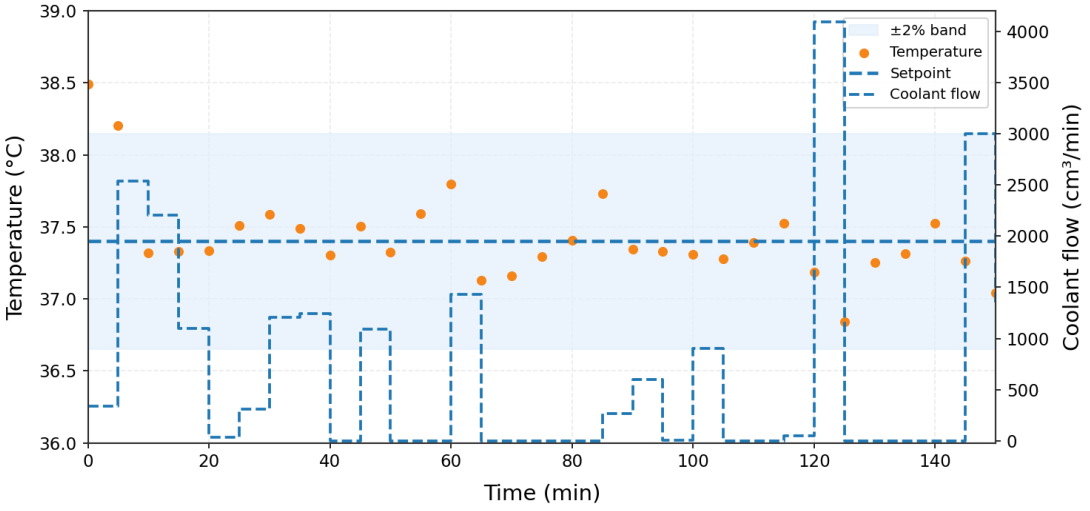

Figure 7. Temperature-Water Flow Control Loop.

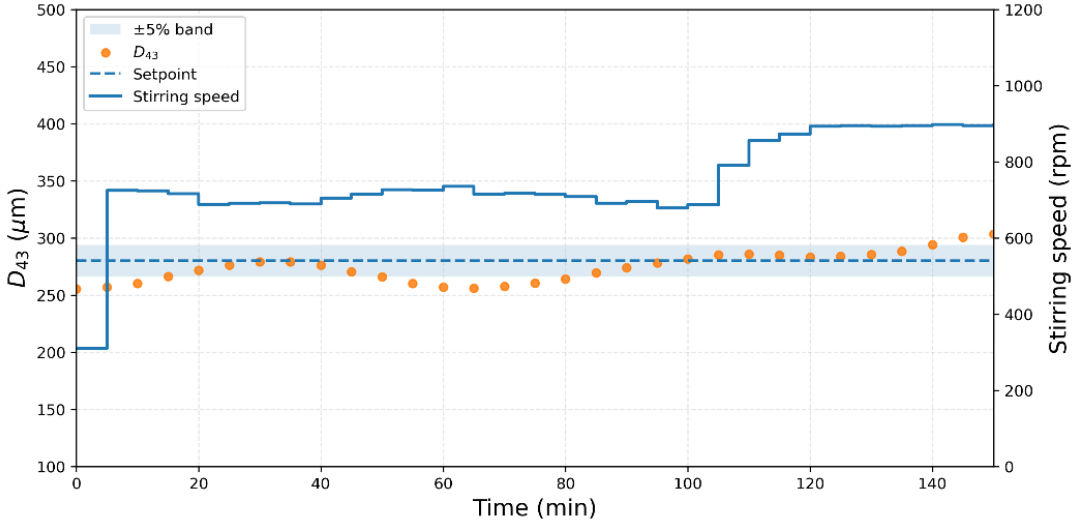

Figure 8. D(4,3)—stirring control loop, with the filter system and new horizons in prediction and control.

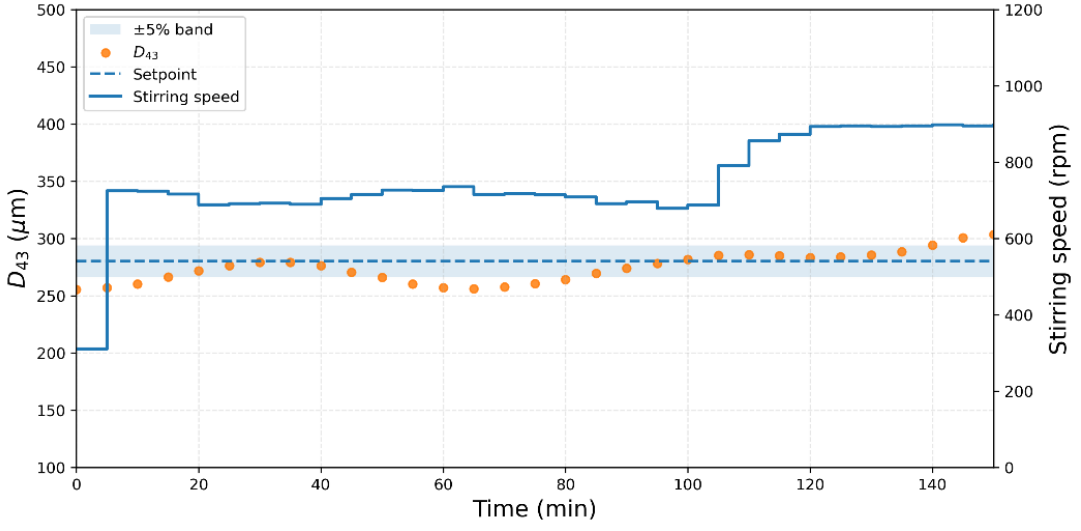

Figure 9. Temperature-Water Flow Control Loop, after the signal filtering has been implemented.

Table 3 MPC controller performance comparison table.

Parameters	Experiment 1	Experiment 2	Experiment 3
IAE D(4,3)	6505.18	5024.12	2201.52
ISE D(4,3)	673379.81	356431.10	37516.54
RMSE D(4,3)	69.06	52.45	14.62
Overshoot D(4,3) (%)	20.13	9.29	8.36
TVu Stirring	2423.01	4237.89	861.46
% within band D(4,3)	29.03	32.26	54.05
IAE Temperature	35.90	42.01	30.25
ISE Temperature	18.93	16.87	8.36
RMSE Temperature	0.356	0.356	0.215
Overshoot Temperature (%)	2.02	2.37	1.34
TVu Water flow	2519.76	28021.06	2898.67
% within band Temperature	96.77	93.55	100

In the third experiment, the impact of digital filtering and the extension of the MPC's prediction and control horizons was subsequently analyzed. Initially, a moving average filter was implemented using five previous measurements to dampen the effect of instrumental noise associated with PAT measurements. Additionally, prediction and control horizons were increased to 85 and 15 respectively. The results obtained under this new configuration are presented in Figures 8 and 9.

The incorporation of digital filtering significantly reduced the extreme fluctuations observed in previous experiments. Figure 8 shows that the dynamics of agitation speed exhibit smoother and less frequent changes, while simultaneously maintaining better control over the CSD. Furthermore, the reduction in fluctuations made it possible to decrease overshoot and increase the operating time within the stability band established for CSD.

Figure 9 shows the thermal performance of the crystallizer. Frequent changes in coolant flow rate decrease and the temperature remains within the ±2% band of the temperature setpoint, ensuring that the process operates within the metastable zone.

Table 3 presents a quantitative analysis of the dynamic performance of the MPC controller for the three configurations evaluated experimentally. Performance metrics such as integral of the absolute value of error (IAE), integral of the square error (ISE), mean square error (RMSE), overshoot, total variation of control action (TVu), and percentage of in-band operation were calculated to compare process stability and the aggressiveness of the control actions implemented.

In experiment 1, a significant oscillatory behavior was observed in the CSD reflected in an overshoot of 20.13% and an RMSE of 69.06 μm. The system remained within the stability band only 29.03% of the time. Although the temperature exhibited more stable behavior, the deviations of D(4,3) indicate that the initial controller configuration generated a poorly damped response. In Experiment 2, the reduction in the weights $W_1^{\Delta U}$ and $W_2^{\Delta U}$ successfully resulted in a lower overshoot of D(4,3) (9.29%) and a lower RMSE. However, the physical effort required by the actuators increased considerably. This effect is particularly prominent in the refrigerant flow loop, where the Total Variation TVu metric rose dramatically to 28,021.06, as detailed in Table 3. This extraordinarily high value is accurate and reflects the aggressive, consecutive corrections made by the control valve. Because the penalty for increases in the control action was minimized, the MPC aggressively adjusted the refrigerant flow to counteract minor thermal deviations, demonstrating that an excessive reduction in weights can significantly increase the operational stress on the physical equipment.

The best overall performance was achieved in experiment 3, where the implementation of digital filtering and the extension of the prediction horizons significantly reduced system oscillations. Under this configuration, the RMSE of D(4,3) decreased to 14.62 μm, and the ISE was reduced by approximately 94% compared to experiment 1. Likewise, the in-band operation percentage increased to 54.05% for CSD and 100% for temperature, while the decrease in TVu confirmed a smoother and more stable control action. These results demonstrate that the incorporation of filtering techniques and proper tuning of the MPC allow for simultaneous improvement in process stability and the operational feasibility of the control system.

Conclusions

A QDMC-type multivariable MPC controller was experimentally implemented in an MSMPR continuous crystallization pilot plant for the ammonium sulfate-water system, using coolant flow and stirring speed in a coordinated manner as manipulated variables for the simultaneous control of temperature and the average diameter D(4,3)

of the crystal size distribution. The internal model based on the population balance method of moments proved to be computationally efficient for real-time execution, adequately capturing the effect of mechanically induced secondary nucleation and allowing the controller to anticipate interactions between the process's thermal and hydrodynamic variables. The experimental results showed that tuning the MPC weights and incorporating digital filtering techniques using time averaging were critical for reducing system oscillations and stabilizing control actions within the physical limits of the actuators. Quantitative performance analysis revealed significant improvements in error and stability metrics, particularly in the reduction of the RMSE and ISE associated with CSD, as well as in the increase in the percentage of operation within the stability band. Furthermore, the decrease in the total variation of the stirring speed confirmed a smoother and operationally viable response for continuous processes. Reference tracking tests demonstrated the proposed scheme's ability to produce crystals with different size specifications while simultaneously maintaining operation within the metastable zone. Finally, the results obtained validate the feasibility of using stirring speed as an active degree of freedom within an experimental MPC scheme for controlling secondary nucleation in MSMPR continuous crystallizers, providing a solid foundation for the development of advanced continuous crystallization systems geared to industrial applications.

Acknowledgements

The authors sincerely appreciate the financial support of the Secretaría de Ciencia, Humanidades, Tecnología e innovación (SECIHTI) for the support of a PhD scholarship.

Nomenclature

A	Heat transfer area between crystallizer and jacket (cm^2)
A_0	Heat transfer area between jacket and surroundings (cm^2)
b	Kinetic order of secondary nucleation with respect to supersaturation (−)
B	Overall secondary nucleation rate (# cm^{-3} min^{-1})
C	Solute concentration in the liquid phase (g solute (g water)$^{-1}$)
C_e	Solute concentration in the feed stream (g solute (g water)$^{-1}$)
C_p	Heat capacity of the solution (cal g^{-1} $°C^{-1}$)
C_{pa}	Heat capacity of the coolant (cal g^{-1} $°C^{-1}$)
C_{Sat}	Saturation concentration (g solute (g water)$^{-1}$)
C_z	Metastable limit concentration (g solute (g water)$^{-1}$)
$D(4,3)$	Volume-weighted mean crystal diameter (De Brouckere mean) (μm)
g	Kinetic order of crystal growth with respect to supersaturation (−)
G	Linear crystal growth rate (cm min^{-1})
h	Exponent for stirring speed in growth kinetics (−)
H_c	Control horizon length (−)
H_p	Prediction horizon length (−)
i	Prediction step index ($i = 0,\ldots,H_p - 1$) (−)
j	Moment index ($j = 0,\ldots,5$)
J	Scalar objective function of the MPC controller (−)
k	Discrete time step / sampling instant (−)
k_b	Secondary nucleation kinetic constant (# $g^{-o}cm^{3o-3}min^{-1}rpm^{-p}$)
k_g	Crystal growth kinetic constant (cm $min^{-1}rpm^{-h}$)
k_v	Volumetric crystal shape factor (−)
M_t	Total crystal mass per unit slurry volume) (g cm^{-3})
n_u	Number of manipulated variables (−)
n_y	Number of output variables (−)
N_r	Stirring speed (rpm)
o	Power exponent for suspension density in nucleation kinetics (−)
p	Power exponent for stirring speed in secondary nucleation kinetics (−)
q	Volumetric coolant flow rate (cm^3 min^{-1})
Q	Volumetric feed flow rate (cm^3 min^{-1})
r	Vector of reference trajectory setpoints (Variable dependent)
S_r	Relative supersaturation ratio (−)
t	Time (min)
T	Slurry temperature in the crystallizer (°C)
T_c	Jacket coolant temperature (°C)
T_e	Feed solution temperature (°C)
T_r	Inlet coolant temperature (°C)
T_∞	Ambient temperature (°C)
u	Manipulated variable vector (Variable dependent)
$u_{\min}, u_{\max}$	Operational lower and upper limits on manipulated variables
U	Overall heat transfer coefficient between crystallizer and jacket (cal $min^{-1}cm^{-2}°C^{-1}$)
U_0	Overall heat transfer coefficient between jacket and surroundings (cal $min^{-1}cm^{-2}°C^{-1}$)

V	Operational crystallizer volume (cm^3)
V_c	Cooling jacket volume (cm^3)
$V^u, V^{\Delta u}, V^y$	Relaxation weight factors for soft constraints (−)
W^y	Weighting factor for output tracking error in MPC cost function (−)
$W^{\Delta u}$	Weighting factor for control move rate in MPC cost function (−)
y	Vector of predicted output variables
$y_{\min}, y_{\max}$	Operational lower and upper limits on output variables

Greek symbols

α	Slack variable for soft constraint relaxation in MPC (−)
ΔH_c	Enthalpy of crystallization (cal g^{-1})
Δu	Vector / increment of control action moves
$\Delta u_{\min}, \Delta u_{\max}$	Lower and upper limits on control action rate of change
ε_e	Liquid volume fraction / voidage in the feed stream (−)
λ	Penalty weight for slack variable in MPC objective function (−)
μ_j	j-th moment of the crystal size distribution ($j = 0, \ldots, 5$) ($cm^j\ cm^{-3}$)
$\mu_{j,e}$	j-th moment of the crystal size distribution in the feed stream ($cm^j\ cm^{-3}$)
ρ	Solution density ($g\ cm^{-3}$)
ρ_a	Coolant fluid density ($g\ cm^{-3}$)
ρ_c	Solid crystal density ($g\ cm^{-3}$)
τ	Mean residence time in the crystallizer (min)

References

Bal, V., & Peters, B. (2020). Crystallization with sinusoidal modulation of stirrer speed: Frequency response analysis and secondary nucleation kinetics. *Crystal Growth & Design*, *21*(1), 235–242. https://doi.org/10.1021/acs.cgd.0c01048

Cao, Y., Acevedo, D., Nagy, Z. K., & Laird, C. D. (2017). Real-time feasible multi-objective optimization based nonlinear model predictive control of particle size and shape in a batch crystallization process. *Control Engineering Practice*, *69*, 1–8. https://doi.org/10.1016/j.conengprac.2017.08.008

Diab, S., & Gerogiorgis, D. (2017). Technoeconomic evaluation of multiple MSMPR crystalliser configurations for continuous cyclosporine crystallisation. *Organic Process Research and Development*, *21*(10), 1571. https://doi.org/10.1021/acs.oprd.7b00225

Enríquez-Torres, L. (2005). *Análisis y control del proceso de cristalización de sulfato de amonio* [Master's thesis, Instituto Tecnológico de Celaya].

Fisher, A. C., Lee, S. L., Harris, D. P., & Buhse, L. F. (2022). An audit of pharmaceutical continuous manufacturing regulatory submissions and outcomes in the US. *International Journal of Pharmaceutics*, *622*, Article 121778. https://doi.org/10.1016/j.ijpharm.2022.121778

Gao, Y., Hou, B., Hu, L., Wang, Y., Jiang, Y., & Wang, J. (2021). Application of PAT-based feedback control approaches in pharmaceutical crystallization. *Crystals*, *11*(3), Article 221. https://doi.org/10.3390/cryst11030221

Larson, M. A., & Mullin, J. W. (1973). Crystallization kinetics of ammonium sulphate. *Journal of Crystal Growth*, *20*(3), 183–191. https://doi.org/10.1016/0022-0248(73)90002-X

Lee, S. L., O'Connor, T. F., Yang, X., Cruz, C. N., Chatterjee, S., Madurawe, R. D., Moore, C. M. V., Yu, L. X., & Woodcock, J. (2015). Modernizing pharmaceutical manufacturing: From batch to continuous production. *Journal of Pharmaceutical Innovation*, *10*(3), 191–199. https://doi.org/10.1007/s12247-015-9215-8

Leeming, R., Mahmud, T., Roberts, K. J., George, N., Webb, J., Simone, E., & Brown, C. J. (2023). Development of a digital twin for the prediction and control of supersaturation during batch cooling crystallization. *Industrial & Engineering Chemistry Research*, *62*(28), 11067-11081. https://doi.org/10.1021/acs.iecr.3c00371

Li, Y., Zhang, Y., & Wang, X. Z. (2020). Secondary nucleation kinetics of AIBN crystallisation in methanol: Online imaging-based measurement and modelling. *Crystals*, *10*(6), Article 506. https://doi.org/10.3390/cryst10060506

Lima, F. A. R. D., de Moraes, M. G. F., Secchi, A. R., & de Souza, M. B. (2022). Development of a recurrent neural networks-based NMPC for controlling the concentration of a crystallization process. *Digital Chemical Engineering*, *5*, 100052. https://doi.org/10.1016/j.dche.2022.100052

Lima, F. A. R. D., de Moraes, M. G. F., Secchi, A. R., de Souza, M. B., & Grover, M. A. (2025). Experimental nonlinear model predictive control of crystal size and yield in batch cooling crystallization enabled by soft sensor and symbolic-based calibration model. *Industrial & Engineering Chemistry Research*, *64*(1), 100–112. https://doi.org/10.1021/acs.iecr.5c03894

Lugo-Martínez, J. R. (2005). *Estudio para la determinación de la zona de saturación metaestable a través del análisis del proceso de nucleación de sulfato de amonio* [Master's thesis, Instituto Tecnológico de Celaya].

Medina-Galván, X. M., Quintana-Hernández, P. A., Reyes-Valadez, J. N., & Fuentes-Cortés, L. F. (2020). Determination of kinetic parameters of nucleation and growth of acetylsalicylic acid crystals in ethanol. *Revista Mexicana de Ingeniería Química*, *19*(1), 445–456. https://doi.org/10.24275/rmiq/Cat1574

Moldoványi, N., Lakatos, B. G., & Blickle, T. (2005). Model predictive control of MSMPR crystallizers. *Journal of Crystal Growth*, *275*(1–2), e1349–e1354. https://doi.org/10.1016/j.jcrysgro.2004.11.170

Mullin, J. W. (2001). *Crystallization* (4th ed.). Butterworth-Heinemann.

Peng, J., Yang, Z., & Lian, P. (2024). Process optimization and crystallization kinetics of ammonium sulfate from wet ammonia-based desulfurization. *Environmental Progress & Sustainable Energy*, *43*(1), Article e14310. https://doi.org/10.1002/ep.14310

Perry, R. H., & Green, D. W. (Eds.). (1997). *Perry's chemical engineers' handbook* (7th ed.). McGraw-Hill.

Qin, S. J., & Badgwell, T. A. (2003). A survey of industrial model predictive control technology. *Control Engineering Practice*, *11*(7), 733–764. https://doi.org/10.1016/S0967-0661(02)00186-7

Quintana-Hernández, P. A., Aguilar-Madera, C. G., & Salcedo-Estrada, L. I. (2017). Development of a fuzzy control system for a non-isothermal continuous crystallizer. *Revista Mexicana de Ingeniería Química*, *16*(2), 663–678.

Reyes-Obando, A. (2012). *Control de cristalizadores continuos por enfriamiento usando control predictivo basado en modelos* [Master's thesis, Instituto Tecnológico de Celaya].

Stoffan, G. N., Lorincz, Z., Pusztai, É., Madarász, L., Tacsi, K., Marosi, G., & Pataki, H. (2024). Development of Continuous Additive-Controlled MSMPR Crystallization by DoE-Based Batch Experiments. *Industrial & Engineering Chemistry Research*, *63*(31), 13709-13722. https://doi.org/10.1021/acs.iecr.4c01933

Sun, F., Liu, T., Song, B., Cui, Y., Nagy, Z. K., & Findeisen, R. (2024). Multi-objective optimization based nonlinear model predictive control of seeded cooling crystallization with application to β form L-glutamic acid. *Chemical Engineering Science*, *299*, Article 120475. https://doi.org/10.1016/j.ces.2024.120475

Tadayon, A., Rohani, S., & Bennett, M. K. (2002). Estimation of nucleation and growth kinetics of ammonium sulfate from transients of a cooling batch seeded crystallizer. *Industrial & Engineering Chemistry Research*, *41*(24), 6181–6193. https://doi.org/10.1021/ie020163r

Tututi-Avila, S. (2010). *Control del proceso de cristalización continuo no-isotérmico empleando lógica difusa* [Doctoral dissertation, Instituto Tecnológico de Celaya].

Wang, L., Zhu, Y., & Gan, C. (2023). Nonlinear model predictive control of crystal size in batch cooling crystallization processes. *Journal of Process Control*, *126*, Article 103020. https://doi.org/10.1016/j.jprocont.2023.103020

Wu, H., Dong, Z., Li, H., & Khan, M. (2015). An integrated process analytical technology (PAT) approach for pharmaceutical crystallization process understanding. *Organic Process Research & Development*, *19*(1), 89–101. https://doi.org/10.1021/op500056a

Xiong, J., Han, J., Zhang, H., Liu, K., Yin, X., Zhang, S., & Chen, J. (2025). Effect of Stirring Paddle Geometry on Nucleation and Growth Crystal Size of Ammonium Sulfate Crystals. *Journal of Chemical & Engineering Data*, *70*(9), 3602-3613. https://doi.org/10.1021/acs.jced.5c00367

Yousuf, M., & Frawley, P. J. (2019). Secondary nucleation from nuclei breeding and its quantitative link with fluid shear stress in mixing. *Organic Process Research & Development*, *23*(5), 926–934. https://doi.org/10.1021/acs.oprd.9b00029

Zhao, B., Zang, H., Zhong, L., Ma, X., Wang, H., Zhang, H., & Li, L. (2023). Review of the application of PAT in the pharmaceutical continuous crystallization process. *Current topics in medicinal chemistry*, *23*(18), 1699-1714. https://doi.org/10.2174/1568026623666230420112709